Title
Strengthening of glass fiber sheets for multi-bolted 1 pultruded GFRP 2 connections: effects of connection type and bolt-tightening force

Author(s)
Phan Viet Nhut / Fengky Satria Yoresta / Tran Quang Duc / MATSUMOTO Yukihiro

Journal
Structures 65

Published
2024-07-07

URL (The Version of Record)
https://doi.org/10.1016/j.istruc.2024.106696

Strengthening of glass fiber sheets for multi-bolted pultruded GFRP connections: effects of connection type and bolt-tightening force

Phan Viet Nhut [1,2*], Fengky Satria Yoresta[1,3], Tran Quang Duc[4], Yukihiro Matsumoto[1]

[1]Department of Architecture and Civil Engineering, Toyohashi University of Technology, Toyohashi, Aichi, Japan.

[2]The University of Danang – University of Technology and Education, Da Nang, Vietnam.

[3]Bogor Agricultural University, Bogor, Indonesia.

[4]Faculty of Construction Economics and Management, Hanoi University of Civil Engineering, Hanoi, Vietnam.

*Correspondence: phan.nhut.viet.hr@tut.jp

Abstract: This study investigated the effects of bolt-tightening forces on the connection strengths of non-strengthened and glass fiber sheet (GFS)-strengthened pultruded glass fiber reinforced polymer (PGFRP) connections through a series of experiments using double-lap and single-lap specimens. A total of 96 specimens (3 specimens for each parameter), half of which were non-strengthened, were tested under tensile loads and four bolt-tightening forces: 0, 5 N.m, 10 N.m, and 20 N.m. The (0°/90°)/chopped strand mat/(0°/90°) lamination was used to bond both PGFRP plates'outside surfaces and improve the connection strengths. The results indicated that maximum failure loads increased with an increase in bolt-tightening forces. However, there were different trends in the maximum failure load changes, depending on the specimen type (non-strengthened or GFS-strengthened specimens; double-lap or single-lap specimens) and bolt-tightening forces. In addition, GFSs could effectively improve PGFRP's connection strengths and ductility performances.

Keywords: GFRP; strengthening; bolted connection; ultimate load; glass fiber sheet; failure mode

1. Introduction

Fiber-reinforced polymer (FRP) materials, such as carbon fiber, aramid, and glass fiber, are commonly used in several fields, ranging from marine, automotive, and aerospace industry to the construction industry, due to their superior properties, which include high strength and durability, a light weight, and high resistance to chemical and corrosion attacks [1-8]. FRP materials' construction applications have focused on two main categories: strengthening aging structures and creating new structures. FRP reinforcement of concrete and steel structures has been extensively researched and reviewed [2, 9-12]. Among FRP materials used in civil engineering fields, glass and carbon fibers have attracted much attention. Carbon fiber is electro-conductive, but glass fiber is an electrical insulation material [2]. Glass fiber is also less expensive than carbon fiber. As a result, using glass fiber in construction has been a notable trend in recent decades. Glass fiber's application in the construction field has also been promoted by a new manufacturing method called the pultrusion method. The pultrusion method can create a wide variety of high-quality pultruded glass fiber-reinforced polymer (PGFRP) profiles with various shapes that are lightweight for transportation and easy to assemble. Using the pultrusion method at a highly industrialized level has contributed to a significant reduction in the cost of PGFRP profiles and facilitated significant potential for their future applications. PGFRP profiles have been used in many real-world construction applications, including bridges and buildings, marine environment structures, emergency structures, cooling towers, pipelines, and guardrail systems [13-18].

FRP members' connections can be bolted, bonded, or bolted–bonded hybrid joints [19]. Bolted connections are popular due to their ease of assembly and disassembly, as well as good load transmission in direct tensile and transverse directions. One of the disadvantages of bolted connections is that stress concentrations can appear around

bolt holes due to fibers' discontinuity [20]. Additionally, because FRP materials have relatively low transversal or shear strengths [21-24], shear-out failures tend to easily occur in PGFRP bolted connections, which reduces joints' load-carrying capacity and ductility. Several researchers have provided solutions to improve PGFRP connections' shear strengths, including carbon nanotubes [25-26], fiber direction optimization using 3D printers [27-28], metal inserts [29], fiber lamination arrangements [30-32], and using glass fiber sheet (GFS) [33-35].

One difficulty when investigating PGFRP connection strength is FRP materials' brittle nature; they generally exhibit the linear behavior of elastic stress and strain until failure [2, 36]. Therefore, FRP materials' failures are usually complex, which is a challenge for researchers. Some researchers have surveyed the effects of several factors, including geometries [34, 37-40], angles between pultrusion direction and loading [41-43], fiber laminations [44-46], and clamping forces [47-49], on the strength of glass fiber-reinforced polymer (GFRP) connections. Many researchers focused on the effects of factors other than clamping forces. Gao et al. [47] estimated clamping forces' effects on the fatigue behavior of pultruded carbon fiber-reinforced polymer joints. They concluded that transversal clamping forces could slow the crack propagation rate and improve the fatigue life. Giannopoulos et al. [48] experimentally investigated the effects of bolt-tightening forces on the fatigue and strength of fiber-reinforced polymer laminations. Their results showed that bolt-tightening forces increased joint strengths. Liu et al. [49] presented experimental and finite element analysis results of the effect of pre-tightening forces on bolted FRP-steel joints. They concluded that joints' load-carrying capacities increased with an increase in pre-tightening forces. Although the above results all concluded that bolt-tightening forces can increase joints' load-carrying capacities, further quantitative studies are necessary to clarify the effects of bolt-tightening forces on PGFRP connections.

This study aimed to investigate GFS' strengthening effects on the connection strengths of double-lap and single-lap multi-bolted PGFRP connections while considering the effects of bolt-tightening forces experimentally. A total of 96 specimens were tested under four types of bolt-tightening forces: 0, 5 N.m, 10 N.m, and 20 N.m. (0°/90°)/chopped strand mat (CSM)/(0°/90°) lamination GFSs (three layers) were used to strengthen PGFRP plates. The (0°/90°) was a two-fiber-orientation glass woven roving sheet, and the CSM was a short-random directional glass fiber sheet. The (0°/90°)/CSM/(0°/90°) GFSs were molded using the vacuum-assisted resin transfer molding (VaRTM) method and bonded to PGFRP plates' outside surfaces.

2. Experimental program

2.1. Materials and specimen types

The experiments' specimens were cut from the main webs of C100B PGFRP profiles (Molymer Matex Co., Ltd., Japan). These channels had 100 × 50 × 6.5 × 6.5 mm cross-sectional areas. PGFRP channels' total thickness was 6.5 mm, which included the outside glass fiber mat (GFM) (approximately 1 mm thick) and the inside unidirectional glass roving (UD) (approximately 5.5 mm thick). Fig. 1 shows a section of C100B PGFRP profiles, PGFRP constitution, and specimen types used in the experiments. Specimen types included two-bolt and four-bolt specimens, and specimens without and with GFS strengthening, as shown in Figs. 1 and 2. The main specimens were 84 mm and 50 mm wide, with four bolts and two bolts, respectively. Double-lap and single-lap specimens were 300 mm and 250 mm long, respectively. All bolts were 8 mm in diameter; bolt holes were 9 mm in diameter. GFSs were attached to both sides of PGFRP plates, in 84 × 80 mm and 50 × 80 mm areas, for four-bolt and two-bolt specimens, respectively. Ratios of the connections' end distance and bolt diameter (e/d) equaled 3d (24 mm) for all connections. Distances between bolts were 4d (32 mm), as per [50]. GFSs were attached to both sides of PGFRP plates using E250 (Konishi, Osaka, Japan), a high-strength adhesive. Its elastic modulus and Poisson's ratio are 3700 MPa and 0.36, respectively. The curing process lasted approximately one week at room temperature (around 20° C) before bolt holes were drilled.

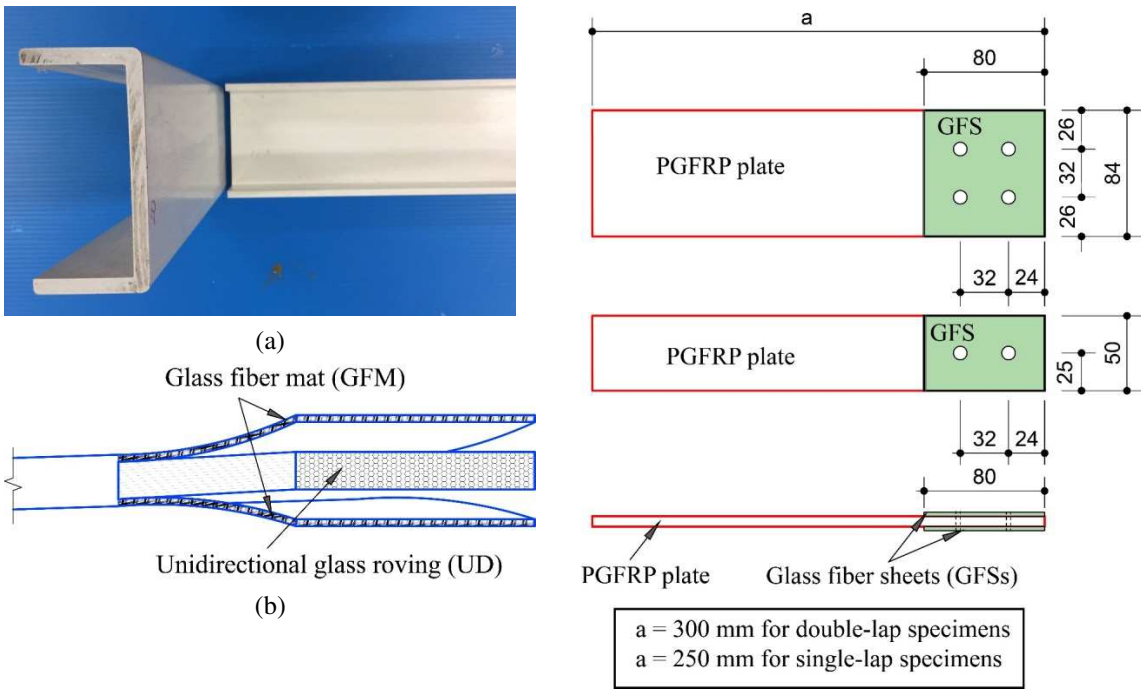

84 **Fig. 1.** Specimen diagrams: (a) C100B profiles, (b) lamination constitution of PGFRP, and (c) specimen types.

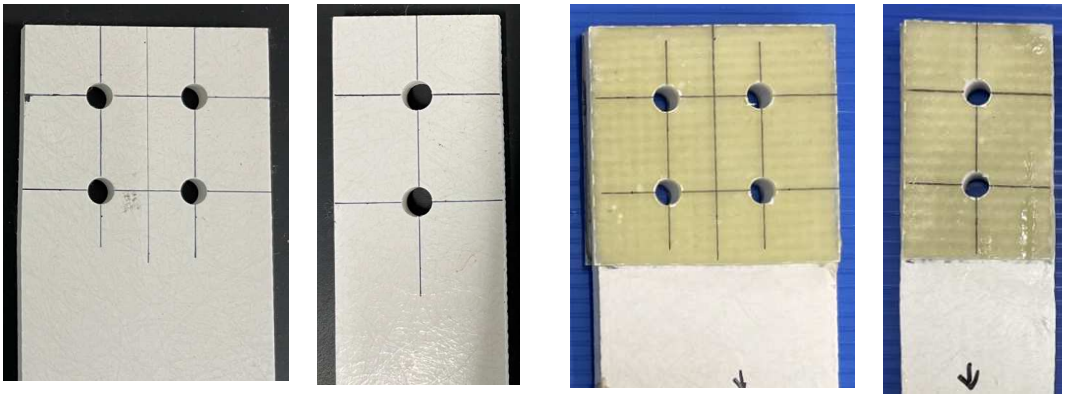

85 **Fig. 2.** PGFRP plates without and with GFS strengthening.

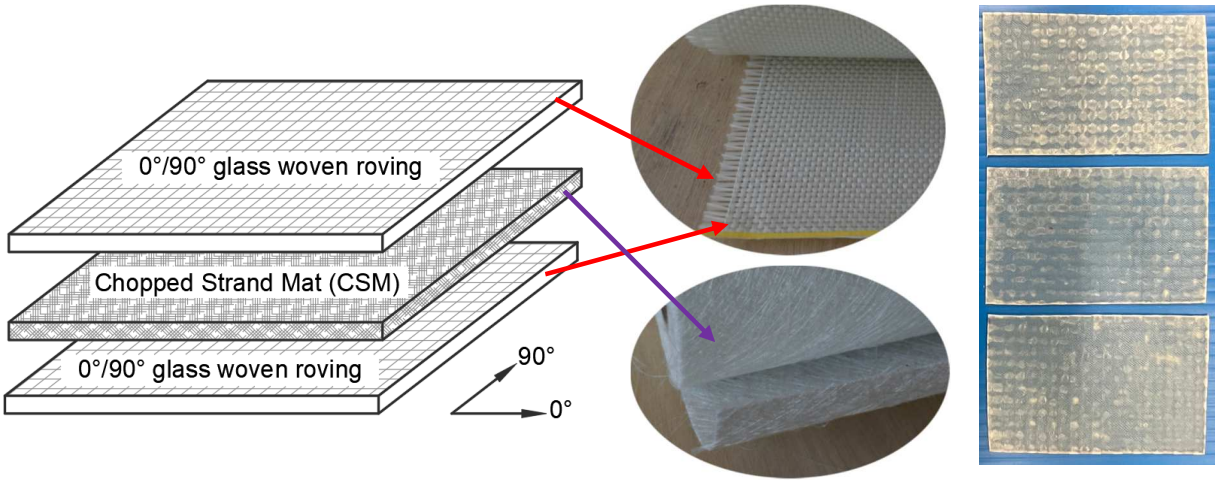

86 **Fig. 3.** GFS used for strengthening: (a) GFS lamination, (b) original GFS layer, and (c) final GFSs after molding
87 and sanding.

Fig. 3 shows the constitutions of GFSs used for strengthening. This study used (0°/90°)/CSM/(0°/90°) GFSs because external (0°/90°) glass woven roving layers can increase GFS-strengthened PGFRP connections' bearing strength and improve their performance [31,35]. The (0°/90°) glass woven roving is an orthotropic material with 0° and 90° fiber directions, whereas CSM can be considered an isotropic material. Because of its short and random fiber directions, CSM can transfer epoxy more easily than (0°/90°) glass woven roving can. This study used (0°/90°) glass woven roving layers (ERW580-554A) and CSM (ECM450-501) that were products of Central Glass Co., Ltd., Tokyo, Japan. The CSM and 0°/90° woven roving weights were 450 (g/m^2) and 580 (g/m^2), respectively. The combination of (0°/90°) glass woven roving on the outside and inside CSM was expected to create a good quality GFS for strengthening. The original GFS layers ((0°/90°) glass woven roving and CSM) were impregnated with E205 epoxy (Konishi, Osaka, Japan) using the VaRTM method [31, 33-35] to create the final GFSs, as shown in Fig. 3. The average thickness of (0°/90°)/CSM/(0°/90°) GFS was approximately 1.26 mm, with an approximate 45% fiber volume content. The Poisson ratio and elastic modulus of E205 adhesive are 0.46 and 1285 MPa, respectively. The final GFSs' surfaces were sanded and then bonded to the PGFRP plates using E250 adhesive.

Table 1 lists all specimens for the double-lap and single-lap tests. There were 96 specimens, half of which were non-strengthened specimens, and three specimens for each parameter. Four types of tightening forces were applied to the connections: 0, 5 N.m, 10 N.m, and 20 N.m. The maximum tightening force of 20 N.m was calculated using the snug-tight condition, as expressed in [50, 51]. The detailed calculation of bolt tightening force is given in Appendix A at the end of the paper. Table 2 lists the mechanical properties of the PGFRP member, UD part, GFM part, and the laminate of GFS, i.e. 0°/90° layer and CSM layer. These properties were tested by Nhut et al. [33,34]. As assumed in the previous studies [33,34], the mechanical properties of the GFM part were equal to those of the CSM layer because both were multi-directional short random fibers. The average shear-out strength of PGFRP plates was calculated by Eq. (1). In this equation, $P_{so.PGFRP}$ is the shear-out failure load of the PGFRP plates, determined by three types of bolt diameters 12 mm, 16 mm, and 20 mm by Nhut et al. [33], e is the end distance from the bolt center to the edge of the PGFRP plate, and t is the thickness of PGFRP plate. Table 3 shows the shear-out strength of the PGFRP plate calculated from the experimental data from Nhut et al. [33].

$$\tau_{so.PGFRP} = \frac{P_{so.PGFRP}}{2et} \quad \textbf{(1)}$$

Table 1. Specimen types for single-lap and double-lap tests.

Specimen name	Type	Describe	Tightening force (N.m)	No. of specimens	No. of bolts
DL-NS2-0 (SL-NS2-0)	DL (SL)	Non-strengthened	0	3 (3)	2
DL-ST2-0 (SL-ST2-0)	DL (SL)	Strengthened	0	3 (3)	2
DL-NS2-5 (SL-NS2-5)	DL (SL)	Non-strengthened	5	3 (3)	2
DL-ST2-5 (SL-ST2-5)	DL (SL)	Strengthened	5	3 (3)	2
DL-NS2-10 (SL-NS2-10)	DL (SL)	Non-strengthened	10	3 (3)	2
DL-ST2-10 (SL-ST2-10)	DL (SL)	Strengthened	10	3 (3)	2
DL-NS2-20 (SL-NS2-20)	DL (SL)	Non-strengthened	20	3 (3)	2
DL-ST2-20 (SL-ST2-20)	DL (SL)	Strengthened	20	3 (3)	2
DL-NS4-0 (SL-NS4-0)	DL (SL)	Non-strengthened	0	3 (3)	4
DL-ST4-0 (SL-ST4-0)	DL (SL)	Strengthened	0	3 (3)	4
DL-NS4-5 (SL-NS4-5)	DL (SL)	Non-strengthened	5	3 (3)	4
DL-ST4-5 (SL-ST4-5)	DL (SL)	Strengthened	5	3 (3)	4
DL-NS4-10 (SL-NS4-10)	DL (SL)	Non-strengthened	10	3 (3)	4
DL-ST4-10 (SL-ST4-10)	DL (SL)	Strengthened	10	3 (3)	4
DL-NS4-20 (SL-NS4-20)	DL (SL)	Non-strengthened	20	3 (3)	4
DL-ST4-20 (SL-ST4-20)	DL (SL)	Strengthened	20	3 (3)	4

DL: double-lap specimens, SL: single-lap specimens

Table 2. The mechanical properties of components.

Laminate	Shear-out strength (MPa)	Bearing strength (MPa)
PGFRP	20.22	-
UD	10.3	260.49
0/90 GFS	-	146.03
CSM GFS	-	199.71
GFM	-	199.71

Table 3. Shear-out strength of PGFRP plate.

Specimen	e (mm)	t (mm)	Failure load (kN)	Shear-out strength (MPa)	Average values (MPa)
M12 bolt	36	6.5	9.83	21.00	
M16 bolt	48	6.5	12.43	19.92	20.22
M20 bolt	60	6.5	15.4	19.74	

2.2. Test diagrams

Figs. 4, 5, and 6 show test diagrams and test setups for double-lap and single-lap specimens, respectively. Tensile loads were applied using a Maekawa universal testing machine with a maximum capacity of 1000 kN. The tensile load was controlled at the average speed of 0.04 kN/second. Loading was applied until specimen failure. The load direction coincided with the PGFRP channels' pultrusion direction. High-strength grade 12.9 bolts M8 × 40 (8 mm bolt diameter) were used for all specimens.

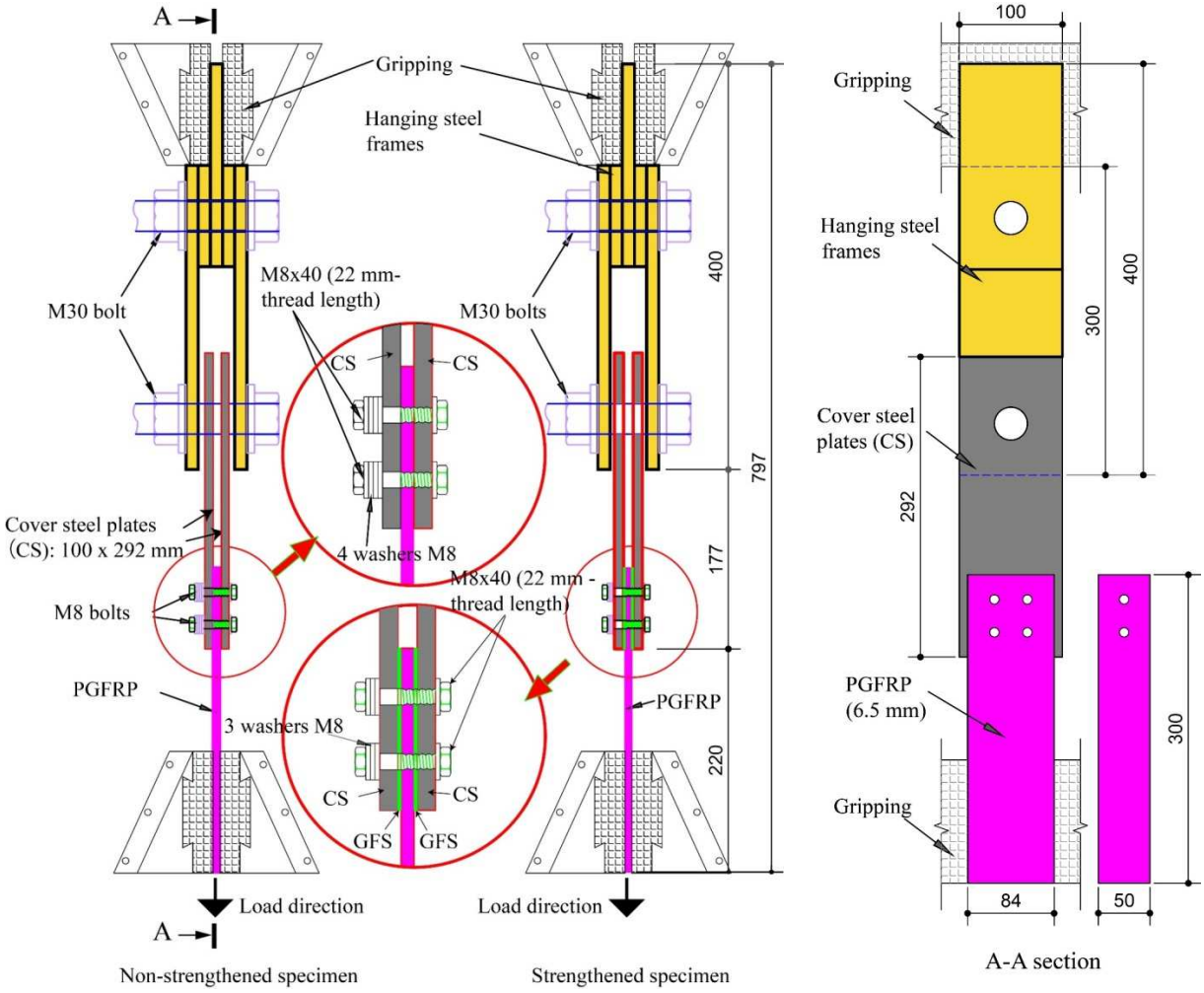

(a) Side view (b) Front view

Fig. 4. Test diagram for double-lap specimens.

The number of washers used was adjusted so that bolt threads were in contact with PGFRP plates in both double-lap and single-lap specimens. Cover steel plates (CS) and steel plates (SP) were contacted directly with PGFRP plates via 4 bolts and 2 bolts (M8 × 40) for double-lap and single-lap specimens, respectively. Tightening forces for PGFRP plates were applied via these bolts. CS in double-lap specimens were 292 × 100 × 9 mm. After being covered by CS and tightened, PGFRP plates in double-lap tests were connected to the testing machine by hanging steel frames, as shown in Fig. 4. For single-lap specimens, PGFRP plates were connected using 16 mm thick SP. To establish the centric tensile load for single-lap specimens, additional steel plates (ASP) were welded to the SP, and molded GFSs (approximately 16 mm thick) were bonded to PGFRP plates using E250 adhesive.

Before applying the tightening forces, all specimens were adjusted the positions (along the tensile direction) so that there were no clearances between steel bolts and PGFRP bolt holes. Meanwhile, PGFRP plates and steel bolts were contacted together from the beginning of the application of load. All bolts were installed without clearances, and the bearing condition was achieved at the early stage of load application. In the next step, a torque wrench measurement device was used to control the tightening force values (5 N.m, 10 N.m, and 20 N.m). The tightening forces were applied several times and in turn for bolt positions in small increments (around 3 N.m) until the required values to prevent the slipping between PGFRP plates and steel surfaces caused by the sudden load. The relative positions of the PGFRP specimens to the CS and SP steel plates' edges were measured carefully after tightening to limit the slip between PGFRP specimens and CS and SP steel plates before and after applying the tightening forces. The positions of PGFRP specimens were checked carefully after applying the tightening forces. If there was any slipping, the tightening forces were removed and applied again.

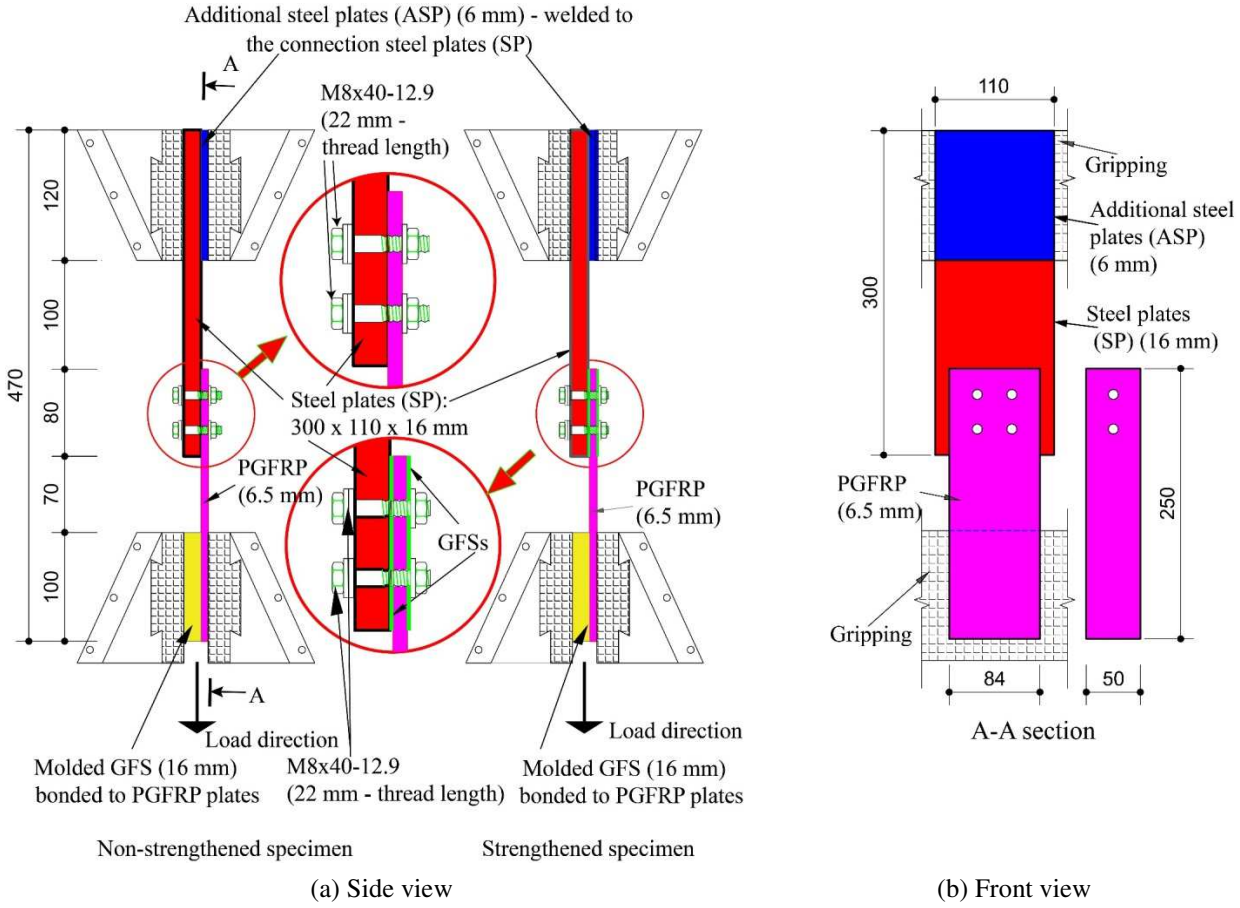

Fig. 5. Test diagram for single-lap specimens.

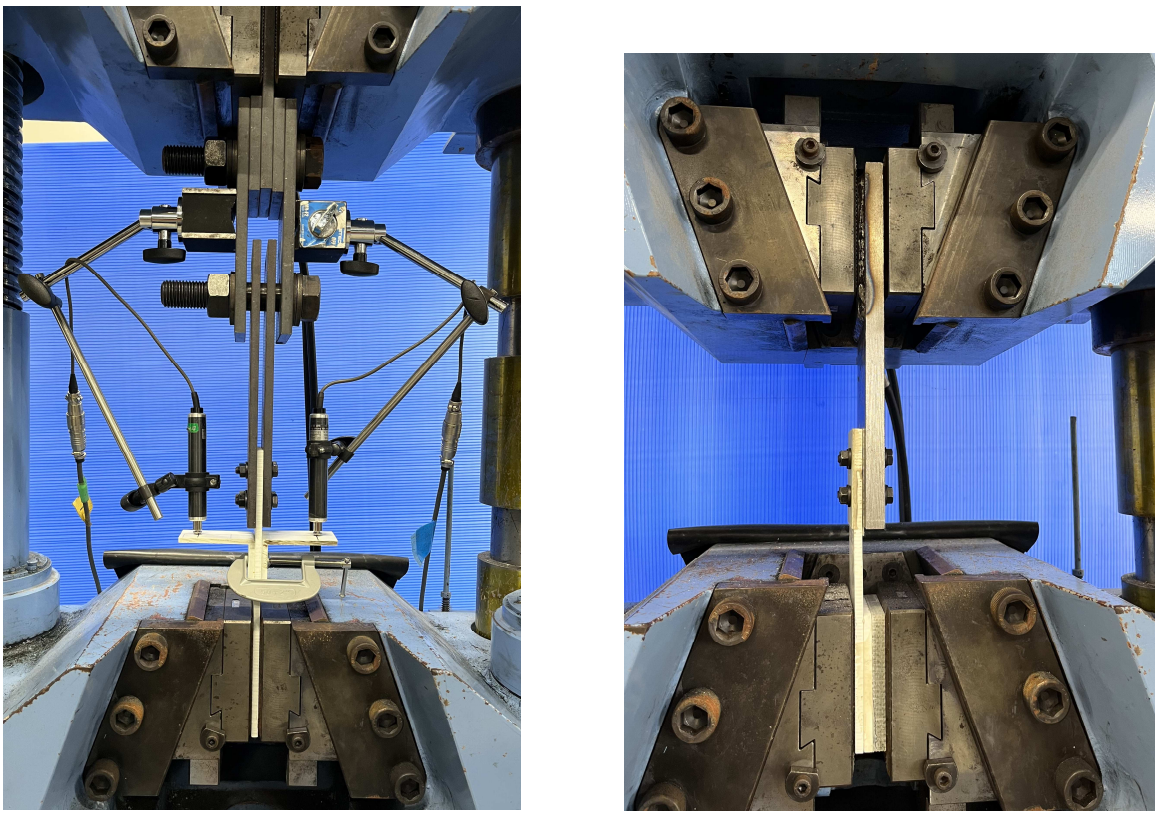

(a) Double-lap specimen (b) Single-lap specimen

Fig. 6. Experimental test setups.

3. Experimental results and discussions

3.1. Failure modes

Figs. 7 and 8 show the typical failure modes of double-lap and single-lap specimens with two bolts and four bolts, respectively; all failure modes are shown in the connections' front and top views. There were generally two types of failure modes. Mode 1 was a shear-out failure throughout the whole thickness of PGFRP plates. Mode 2 was a combination of shear-out failures in the UD section (5.5 mm) and bearing failures in the GFM and GFS sections. Mode 1 occurred in non-strengthened specimens, whereas Mode 2 occurred in GFS-strengthened specimens. The shear-out length of Mode 1 failures developed from the second bolts to the connections' edges. The shear-out areas of non-strengthened specimens without tightening forces tended to be smaller than those of non-strengthened specimens with tightening forces (e.g., DL-NS2-0, SL-NS2-0, DL-NS4-0, and SL-NS4-0). In GFS-strengthened specimens, bearing failures could easily be identified via GFSs' out-of-plane deformation. When tightening forces were 0, GFSs' out-of-plane deformations were larger than those to which tightening forces were applied, as specimens' surfaces were subjected to the compression pressure of tightening forces. Bearing failures were still found in GFSs with tightening forces; however, out-of-plane deformations occurred more slowly while ultimate loads increased. GFSs' out-of-plane deformations were also larger for single-lap specimens, because of their bending behaviors. Figs. 7 and 8 show that shear-out failures only appeared in the UD sections of GFS-strengthened specimens. In single-lap specimens, SL-ST2-10 and SL-ST2-20, debonding failure occurred on one side of the specimens (between GFM and UD sections) at the final step when loading decreased.

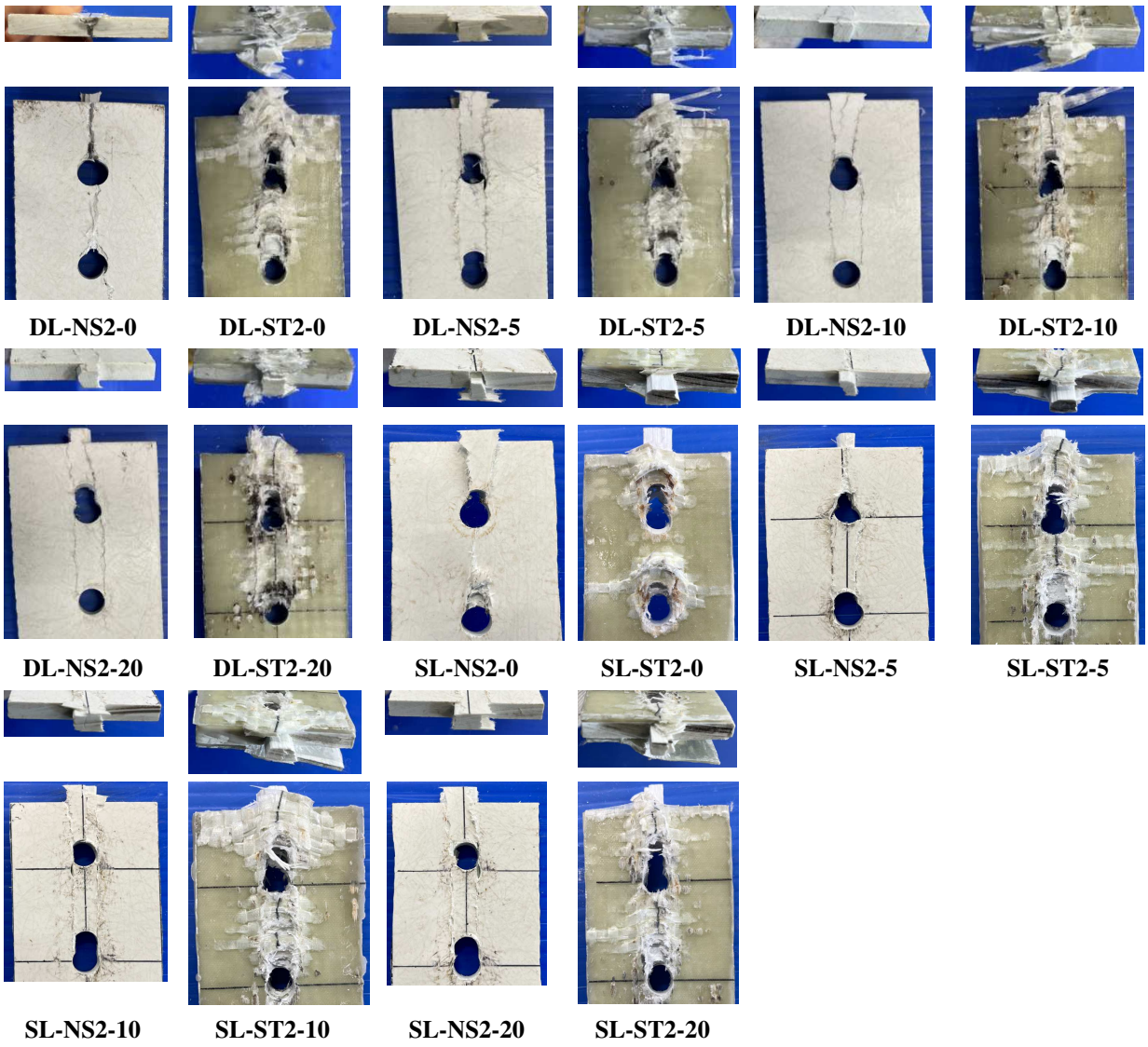

Fig. 7. Typical failure modes of single-lap and double-lap specimens with two bolts.

3.2. Load and displacement relations

Figs. 9 and 10 present the load and crosshead displacement relations of double-lap and single-lap specimens, respectively. There were differences in the behaviors of non-strengthened and GFS-strengthened specimens. The failure behaviors of non-strengthened specimens in both double-lap and single-lap tests were generally the same, regardless of the impact of bolt-tightening forces. These specimens' maximum loads suddenly dropped after the PGFRP plates' shear-out failures. In contrast, there were some changes in the load-displacement relations of GFS-strengthened specimens concerning types of connections. Regarding the effects of the bolt number, four-bolt specimens in GFS-strengthened connections had signs of higher stability in high-load areas compared to two-bolt specimens when load values had smaller variations in four-bolt specimens. Double-lap specimens in GFS-strengthened connections also performed better than single-lap specimens did when maximum loads were maintained in longer displacements, especially in four-bolt specimens. Overall, all GFS-strengthened specimens had better ductility performances compared to non-strengthened specimens when loadings were maintained at maximum values for a longer time.

3.3. Effects of bolt-tightening forces

Tables 4 to 7 show maximum loads for all connection types and the effects of bolt-tightening forces on double-lap and single-lap connections with and without GFS strengthening. The maximum coefficient of variation (C.O.V.) for the ultimate loads was found in the SL-NS2-10 specimen (14.7%). This maximum C.O.V was acceptable

compared to the C.O.V in the previous results of Nhut et al. [33,34]. Load increases presented in these tables were calculated based on increased loads by applying tightening forces compared to 0 tightening forces. Fig. 11 shows the load and tightening force relations of all specimens and load-increasing levels of connections after they were strengthened using GFSs.

In general, maximum failure loads increased as tightening forces increased. There were differences in the load changes of double-lap and single-lap specimens. Without tightening forces, maximum loads were approximately the same in both single-lap and double-lap specimens. The maximum variation was 9.71% in specimens SL-ST2-0 and DL-ST2-0. The reason for this variation was a small loading transfer eccentricity in single-lap specimens.

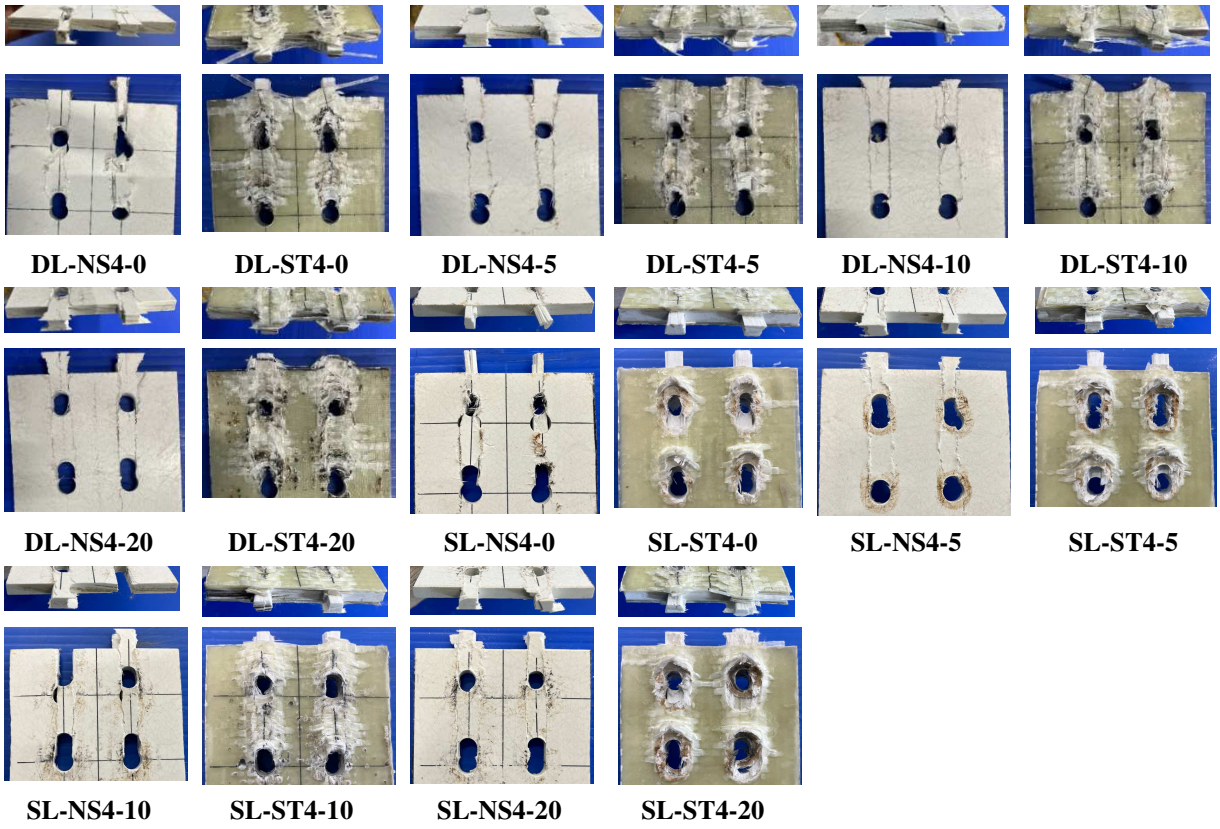

Fig. 8. Typical failure modes of single-lap and double-lap specimens with four bolts.

When tightening forces increased, changes in maximum loads exhibited different trends, depending on the connection type. In non-strengthened specimens, connections' maximum loads were approximately the same for 5 N.m and 10 N.m bolt-tightening forces. However, when the tightening force was increased to 20 N.m, larger variations were found between the maximum failure loads of double-lap and single-lap non-strengthened specimens (e.g., 29.20 % between SL-NS2-20 and DL-NS2-20, and 32.711% between SL-NS4-20 and DL-NS4-20). As a result, high bolt-tightening forces (20 N.m) could provide better performance for double-lap connections compared to single-lap connections in non-strengthened specimens. For GFS-strengthened specimens with two bolts, there were no significant dissimilarities between double-lap and single-lap specimens; the maximum variation was 12.03% between specimens SL-ST2-10 and DL-ST2-10. In four-bolt GFS-strengthened specimens, double-lap specimens' maximum loads rose by approximately 18.8 % compared with those of single-lap specimens. In general, differences were small in GFS-strengthened connections with two bolts when bolt-tightening forces were increased. In addition, maximum loads increased in double-lap GFS-strengthened specimens compared with single-lap specimens when bolt-tightening forces were 10 N.m and 20 N.m.

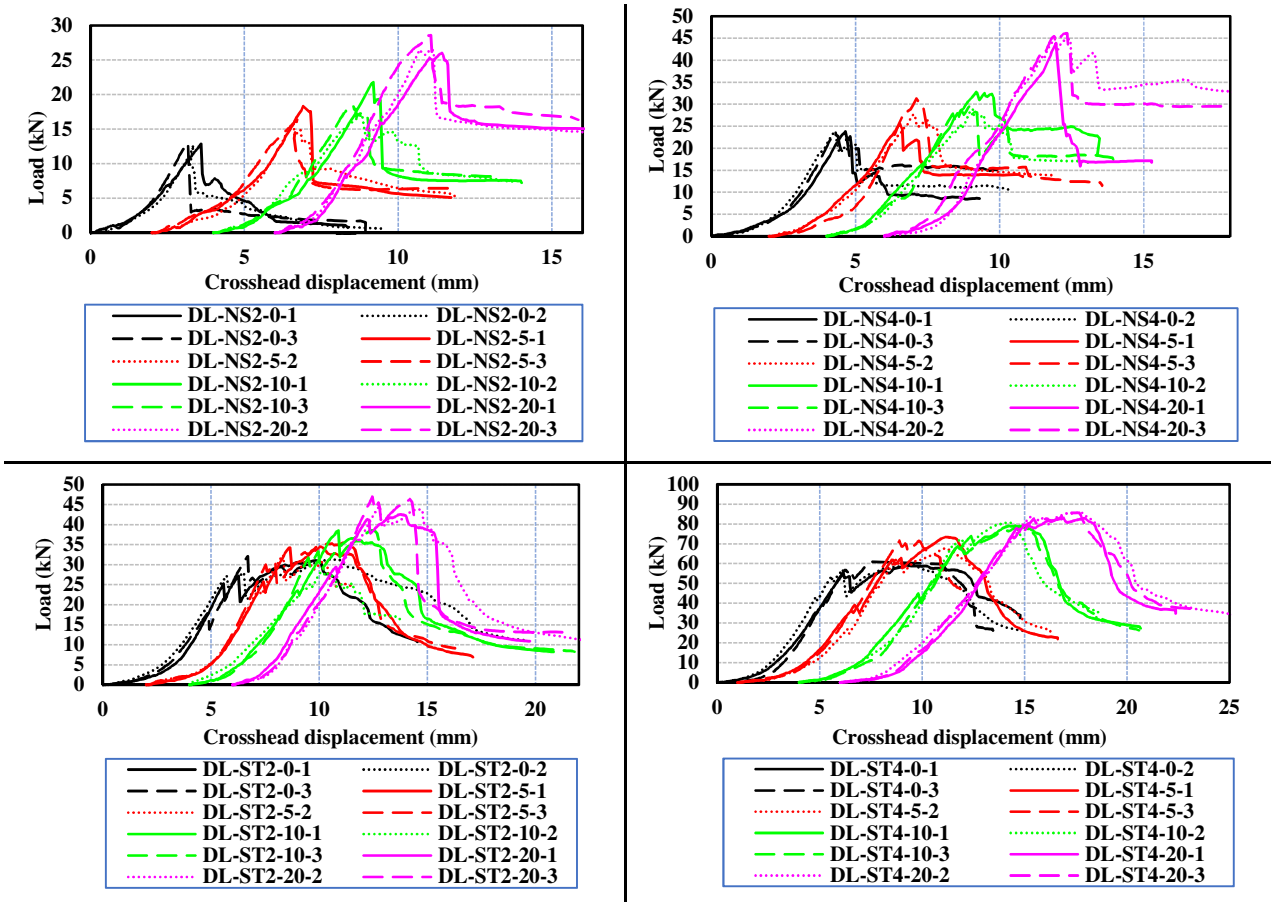

Fig. 9. Load–crosshead displacement relations of double-lap specimens.

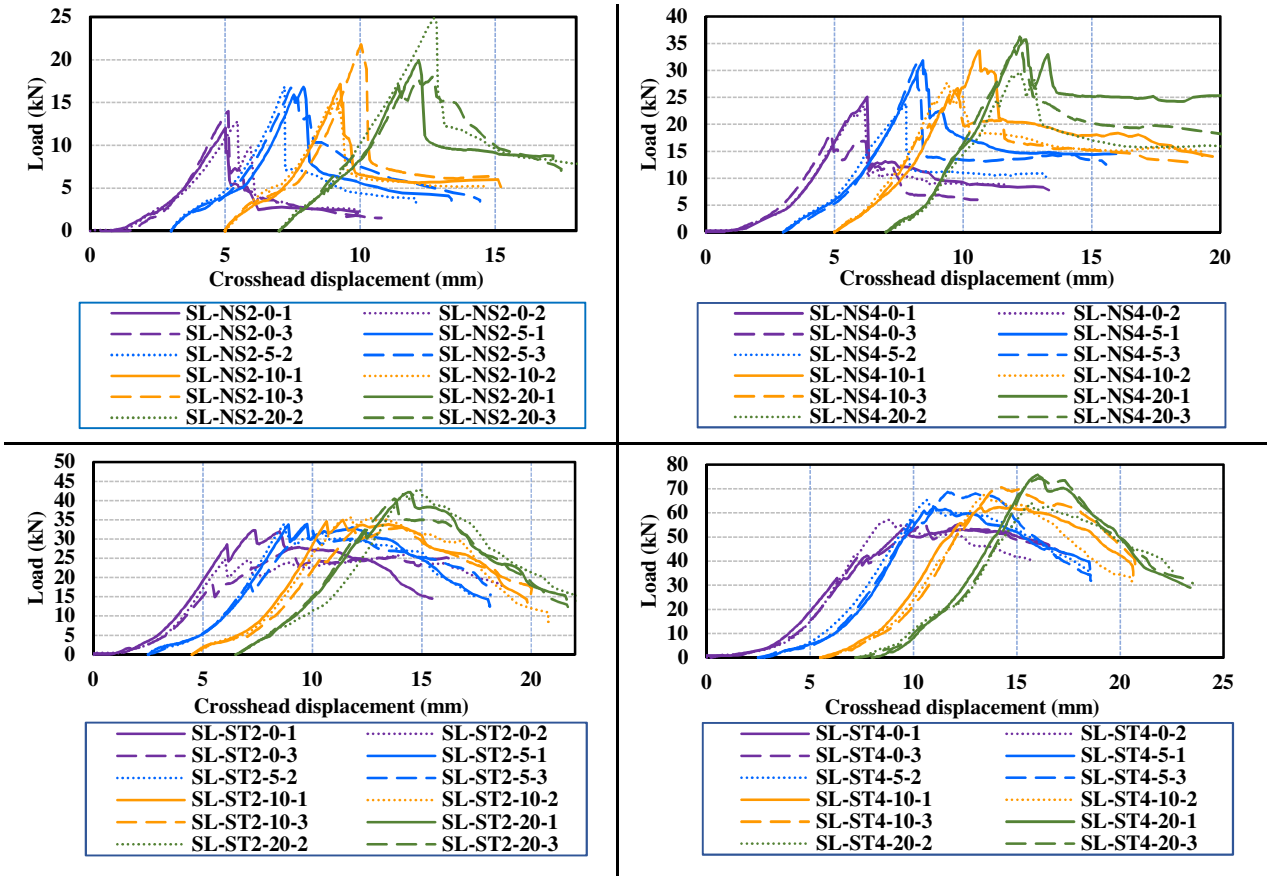

Fig. 10. Load–crosshead displacement relations of single-lap specimens.

Table 4. Effects of bolt-tightening forces on non-strengthened single-lap and double-lap specimens with two bolts.

Parameters	No.	SL-NS2-0 / DL-NS2-0	SL-NS2-5 / DL-NS2-5	SL-NS2-10 / DL-NS2-10	SL-NS2-20 / DL-NS2-20
Tightening forces (N.m)		0 / 0	5 / 5	10 / 10	20 / 20
Loads (kN)	1	12.05 / 12.88	16.81 / 18.33	17.17 / 21.79	19.95 / 26.01
	2	12.80 / 12.70	16.88 / 15.84	15.46 / 17.15	24.88 / 26.56
	3	14.00 / 12.98	16.71 / 16.39	21.78 / 18.42	17.99 / 28.58
Average maximum loads (kN)		12.95 / 12.85	16.80 / 16.85	18.14 / 19.12	20.94 / 27.05
Variation of SL and DL*		-0.76%	0.35%	5.43%	29.20%
C.O.V		0.062 / 0.009	0.004 / 0.063	0.147 / 0.102	0.138 / 0.041
Load increase levels (%)		---	29.71 / 31.16	40.06 / 48.81	61.68 / 110.49

* Variation between average maximum loads of double-lap and single-lap specimens

Table 5. Effects of bolt-tightening forces on GFS-strengthened single-lap and double-lap specimens with two bolts.

Specimen	No.	SL-ST2-0 / DL-ST2-0	SL-ST2-5 / DL-ST2-5	SL-ST2-10 / DL-ST2-10	SL-ST2-20 / DL-ST2-20
Tightening forces (N.m)		0 / 0	5 / 5	10 / 10	20 / 20
Loads (kN)	1	32.26 / 31.07	33.92 / 34.46	34.92 / 38.50	42.20 / 42.54
	2	26.06 / 31.37	34.05 / 32.40	35.63 / 38.91	42.93 / 44.61
	3	27.83 / 32.08	33.83 / 35.45	32.97 / 38.55	40.48 / 46.97
Average maximum loads (kN)		28.72 / 31.51	33.93 / 34.10	34.51 / 38.66	41.87 / 44.71
Variation of SL and DL*		9.71%	0.49%	12.03%	6.78%
C.O.V		0.091 / 0.013	0.003 / 0.037	0.033 / 0.005	0.025 / 0.040
Load increase levels (%)		---	18.16 / 8.23	20.15 / 22.69	45.80 / 41.90

* Variation between average maximum loads of double-lap and single-lap specimens

Table 6. Effects of bolt-tightening forces on non-strengthened single-lap and double-lap specimens with four bolts.

Specimen	No.	SL-NS4-0 / DL-NS4-0	SL-NS4-5 / DL-NS4-5	SL-NS4-10 / DL-NS4-10	SL-NS4-20 / DL-NS4-20
Tightening forces (N.m)		0 / 0	5 / 5	10 / 10	20 / 20
Loads (kN)	1	25.07 / 23.82	31.83 / 25.55	33.67 / 32.78	35.72 / 43.91
	2	23.43 / 23.55	23.90 / 27.61	27.72 / 28.90	29.70 / 44.86
	3	18.28 / 23.78	31.37 / 31.31	26.78 / 29.49	36.23 / 46.12
Average maximum loads (kN)		22.26 / 23.72	29.03 / 28.15	29.39 / 30.39	33.88 / 44.96
Variation of SL and DL*		6.56%	-3.02%	3.40%	32.71%
C.O.V		0.130 / 0.005	0.125 / 0.085	0.104 / 0.056	0.087 / 0.020
Load increase levels (%)		---	30.44 / 18.71	32.05 / 28.13	52.23 / 89.58

* Variation between average maximum loads of double-lap and single-lap specimens

Table 7. Effects of bolt-tightening forces on GFS-strengthened single-lap and double-lap specimens with four bolts.

Specimen	No.	SL-ST4-0 / DL-ST4-0	SL-ST4-5 / DL-ST4-5	SL-ST4-10 / DL-ST4-10	SL-ST4-20 / DL-ST4-20
Tightening forces (N.m)		0 / 0	5 / 5	10 / 10	20 / 20
Loads (kN)	1	53.53 / 59.18	62.38 / 73.44	62.38 / 79.07	75.85 / 83.03
	2	57.21 / 59.38	65.38 / 67.69	67.85 / 80.93	64.18 / 85.78
	3	55.43 / 60.94	68.67 / 71.48	70.72 / 78.93	74.34 / 85.67
Average maximum loads (kN)		55.39 / 59.83	65.48 / 70.87	66.99 / 79.64	71.46 / 84.83
Variation of SL and DL*		8.02%	8.23%	18.89%	18.71%
C.O.V		0.027 / 0.013	0.039 / 0.034	0.052 / 0.011	0.073 / 0.015
Load increase levels (%)		---	18.21 / 18.44	20.94 / 33.10	29.01 / 41.78

* Variation between average maximum loads of double-lap and single-lap specimens

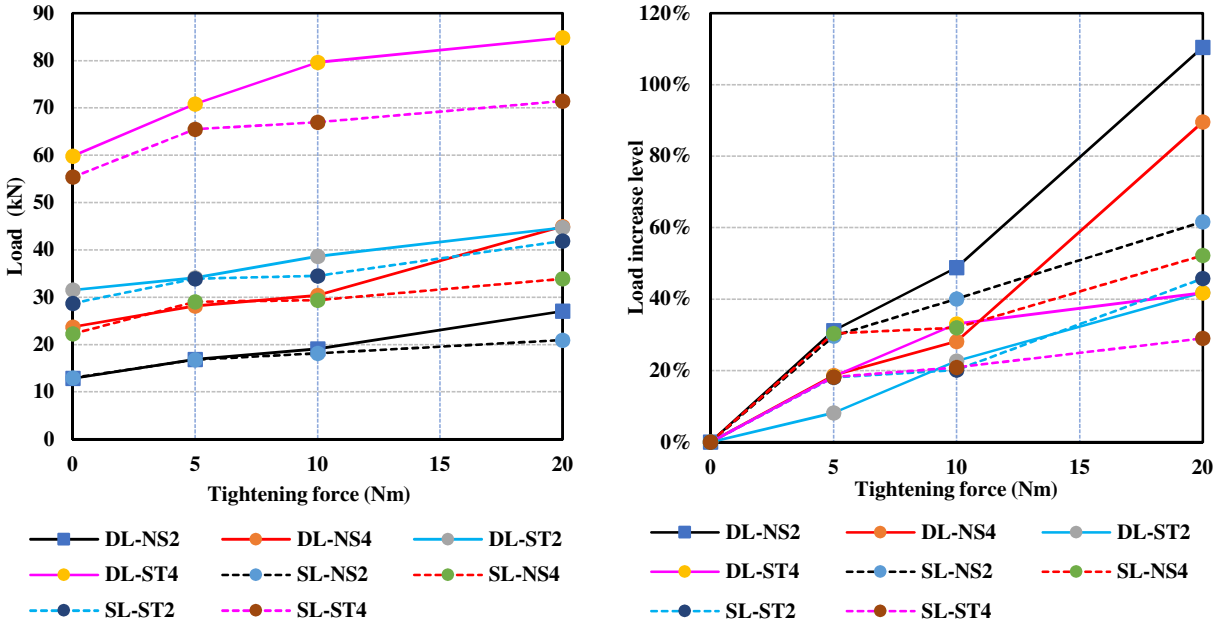

227 **Fig. 11.** Load–tightening force relations and load-increasing levels after being strengthened with GFSs.

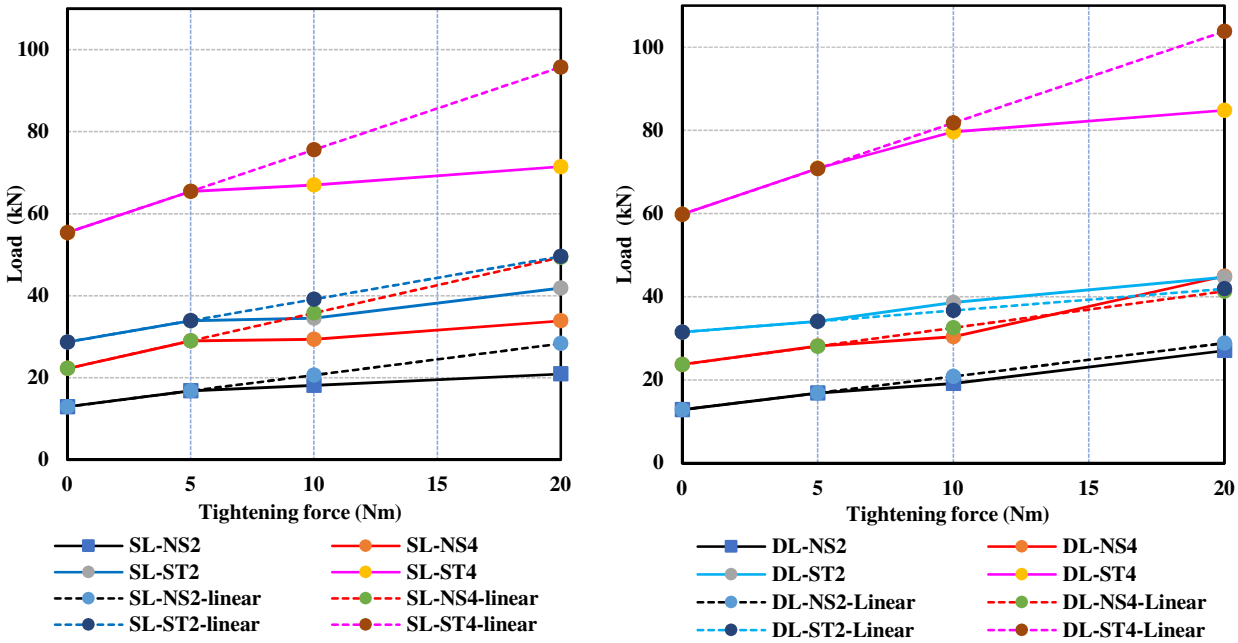

(a) (b)

228 **Fig. 12.** Load–tightening force relations in (a) single-lap specimens and (b) double-lap specimens.

229 Fig. 12 shows the load and bolt-tightening force relations in both double-lap and single-lap specimens. In these
230 graphs, dash lines are linear extensions of failure load values of connections without bolt-tightening forces and 5
231 N.m bolt-tightening forces. Regarding the relationship between load increase and bolt-tightening force increments,
232 there were several differences between double-lap and single-lap specimens. For double-lap non-strengthened
233 specimens and GFS-strengthened two-bolt specimens, increasing maximum loads changed at approximately the
234 same rate as the tightening force increment did. On the other hand, increasing maximum loads were not linearly
235 commensurate with the increase in tightening forces for GFS-strengthened four-bolt double-lap specimens. The
236 linear increase in PGFRP connections' ultimate loads could be predicted approximately correctly when increasing
237 tightening forces on double-lap specimens, except for DL-ST4 specimens with high tightening forces (20 N.m).
238 There were large variations between continuous line graphs and dash line graphs for single-lap specimens when

bolt-tightening forces were increased to 10 N.m and 20 N.m. There were no extreme differences in load increases for 5 N.m, 10 N.m, and 20 N.m bolt-tightening forces in single-lap specimens. The linear increase in PGFRP connections' ultimate loads could not be predicted for single-lap connections because single-lap connections tended to bend after tensile loads were applied, and friction surfaces and friction loads changed as a result.

3.4. GFSs' strengthening effects on PGFRP connections

Table 8 indicates GFSs' strengthening effects for PGFRP connections in double-lap and single-lap tests. Increased ratios of maximum loads were calculated by dividing the maximum loads of GFS-strengthened specimens by those of non-strengthened specimens having the same geometries corresponding to different bolt-tightening forces. Table 8 shows that GFSs could improve PGFRP connections' load-carrying capacities by approximately 1.65 to 2.5 times for two-bolt specimens and approximately 1.9 to 2.5 times for four-bolt specimens.

Table 8. Increasing ratios of maximum loads of GFS-strengthened connections (times).

Specimen	Bolt-tightening forces (N.m)			
	0	5	10	20
SL with two bolts	2.22	2.02	1.90	2.00
SL with four bolts	2.49	2.26	2.28	2.11
DL with two bolts	2.45	2.02	2.02	1.65
DL with four bolts	2.52	2.52	2.62	1.89

DL and SL: double-lap and single-lap specimens, respectively

Fig. 11 and Tables 4 to 7 show the load-increasing levels of all GFS-strengthened connections with various bolt-tightening forces. Load-increasing levels were determined according to the increase in maximum loads when bolt-tightening forces were applied compared with 0-tightening forces. When increasing tightening forces, load-increasing levels in GFS-strengthened specimens were smaller than those in non-strengthened specimens. Therefore, GFSs enabled better PGFRP connection performance because GFSs restricted bolt-tightening forces' effects on connection strengths. This was better for connections because tightening forces could be loosened during structures' working conditions. Moreover, according to the load and displacement relations illustrated in Figs. 9 and 10, GFS-strengthened specimens had better ductility performances compared with non-strengthened specimens, especially in DL-ST4 specimens.

4. Theoretical prediction of the failure loads of multi-bolted PGFRP connections with 0 tightening forces

In this study, the failure loads of multi-bolted PGFRP connections with 0 tightening forces are predicted by the following theoretical equations (Eqs. (2) – (7)). There were generally two types of failure modes, Mode 1 and Mode 2. Mode 1 occurred in non-strengthened specimens, in which shear-out failure appeared in the whole thickness of PGFRP plates. Mode 2 was identified in GFS-strengthened specimens, where shear-out failures occurred in the UD part, and bearing failures appeared in the GFM and GFS parts. Eqs. (2) and (3) express the predicted failure loads for Mode 1 and Mode 2, respectively.

Mode 1:
$$P_1 = \sum R_{so\cdot PGFRP} \tag{2}$$

Mode 2:
$$P_2 = \sum R_{so.UD} + \sum R_{bi} \tag{3}$$

where $R_{so\cdot PGFRP}$ is the shear-out failure load per bolt line of the non-strengthened PGFRP connections, $R_{so.UD}$ is the shear-out failure load per bolt line of the UD part of GFS-strengthened specimens, R_{bi} is the bearing failure load of the components (e.g. GFM and GFS parts). The values of $R_{so\cdot PGFRP}, R_{so.UD}, R_{bi}$ are determined by Eqs. (4) - (6).

$$R_{so\cdot PGFRP} = 2\beta\tau_{so.PGFRP} t l_{so} = 2\beta\tau_{so.PGFRP} t\left(e - \phi/2 + s\right) \tag{4}$$

$$\beta(\%) = 1 - \alpha(\%) \quad (5)$$

$$R_{so.UD} = 2\beta l_{so}(t_{UD} + d)\tau_{so.UD} = 2\beta\left(e - \phi/2 + s\right)(t_{UD} + d)\tau_{so.UD} \quad (6)$$

$$R_{bi} = \sum \beta n t_i d F_{bi} \quad (7)$$

where $\tau_{so.PGFRP}$ is the shear-out strength of PGFRP plates, which is determined by Eq. (1) (section 2.1); $l_{so} = \left(e - \phi/2 + s\right)$ is the shear-out length of PGFRP plates (referred from [52]); e is the end distance from the first bolt row to the edge of the specimens (e = 24 mm); s is the distance between two bolt row in tensile load direction (s = 32 mm); ϕ is the bolt-hole diameter (ϕ = 9 mm); t is the thickness of PGFRP plates; $2l_{so}(t_{UD} + d)$ is the shear-out areas of the UD parts in GFS-strengthened specimens; $\tau_{so.UD}$ is the shear-out strength of the UD parts; n is the number of bolts of the specimens; t_i is the thickness of bearing components (GFM and GFS parts); d is the diameter of the bolt (d = 8 mm); F_{bi} is the bearing strength of the components (GFM and GFS parts), determined in section 2.1; α is the load reduction percentage between non-thread bolted and thread-bolted connections.

The bearing strength of the GFS part can be calculated by the total bearing strength of two components, i.e. 0°/90° GFS and CSM GFS. The total thickness of the GFS part on one side is around 1.26 mm, in which the thickness of 0°/90° GFS is around 0.76 mm and the thickness of CSM GFS is around 0.48 mm. These thicknesses are measured by the molding of separately 0°/90° GFS and CSM GFS with the same VaRTM method and materials. The parameter α is considered because the shear-out strength and bearing strength of components determined in section 2.1 were from the previous studies [33,34] with non-thread bolts. In contrast, the PGFRP plates in this study suffered from thread areas of bolts.

The effects of α were determined by the following experiments. Fig. 13 shows the tests to investigate the effects of bolt thread on the strengths of PGFRP connections. The double lap tests were conducted with four types of specimens, i.e. non-strengthened specimens with two and four bolts (NT-DL-NS2-0 and NT-DL-NS4-0) and GFS-strengthened ones with two and four bolts (NT-DL-ST2-0 and NT-DL-ST4-0). The sizes of the specimens were the same as the main specimens in the main tests (section 2.1). Longer bolts M8 x 80 were used for the specimens without bolt thread in the connection parts.

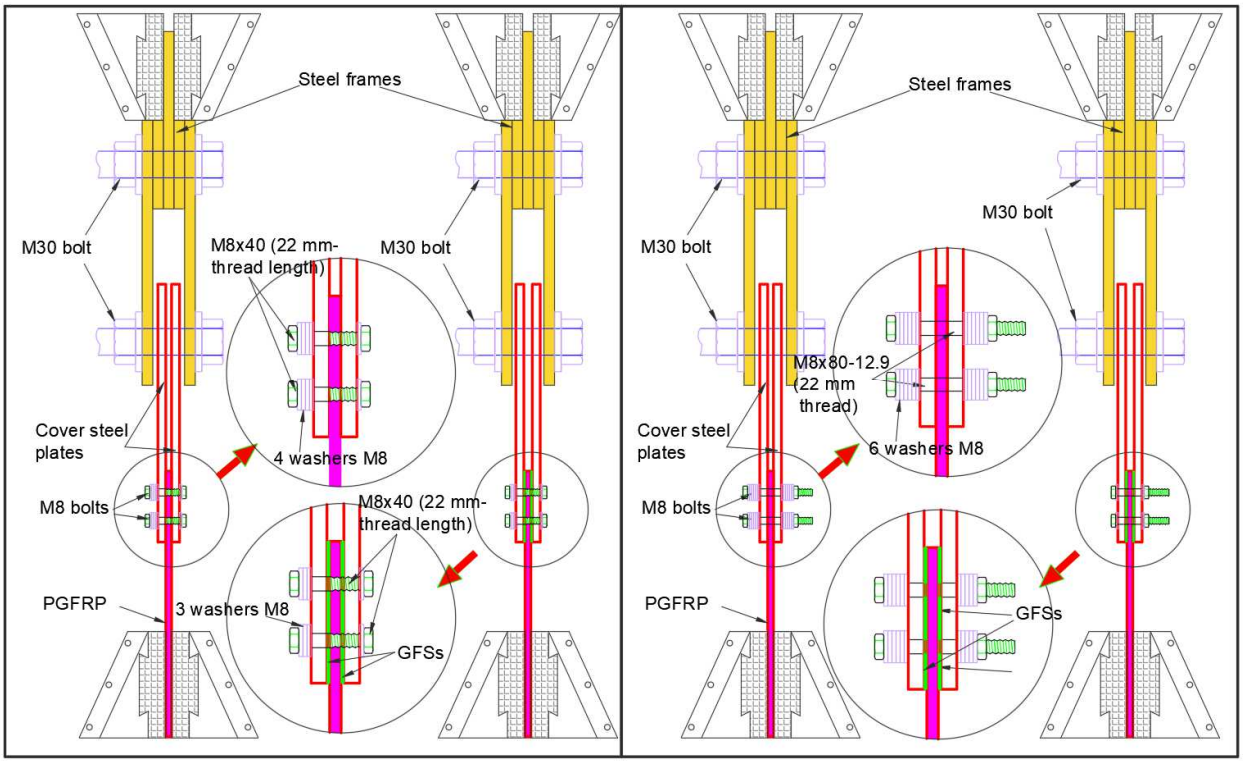

(a) (b)

Fig. 13. Bolt thread tests: (a) connection with bolt thread and (b) without bolt thread in PGFRP connection.

Fig. 14 and Table 9 indicate the load-displacement relations and maximum failure load obtained from the tests. Table 10 shows the comparison of maximum failure loads of the specimens with and without bolt threads. The results indicated that the threads had certain effects on the connection strengths of non-strengthened specimens, whereas these effects were very small in GFS-strengthened specimens. The maximum failure loads of non-strengthened specimens with thread bolts were smaller than those of non-thread bolts with a decreasing percentage of around 9% and 7% for two and four-bolt specimens, respectively. It can be seen that GFS could create better performance for the specimens having thread bolts when the maximum failure loads of these specimens were almost the same as non-thread bolt specimens. Because the effects of bolt threads on the connection strength of PGFRP connections were not too high, the factor α in the experiments of double lap tests was applied for the single lap specimens as well to simplify the estimation.

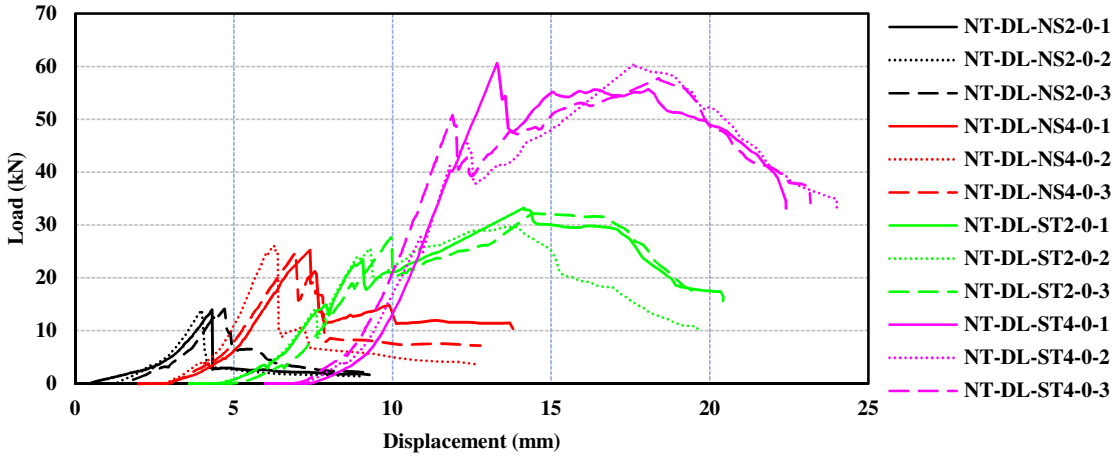

Fig. 14. Load-displacement relations of PGFRP connections without bolt thread in the connections.

Table 9. Results of bolt thread effect tests

Specimen		NT-DL-NS2-0	NT-DL-NS4-0	NT-DL-ST2-0	NT-DL-ST4-0
Maximum loads (kN)	1	13.98	25.26	33.24	60.61
	2	13.92	25.98	29.62	60.55
	3	14.13	24.88	32.18	57.75
Average maximum loads (kN)		14.01	25.37	31.68	59.64
C.O.V		0.006	0.018	0.048	0.022

Table 10. Effect of bolt thread on the ultimate loads of PGFRP connection

Specimen	NT-DL-NS2-0	NT-DL-NS4-0	NT-DL-ST2-0	NT-DL-ST4-0
Ultimate load (kN)	14.01	25.37	31.68	59.64
Specimen	DL-NS2-0	DL-NS4-0	DL-ST2-0	DL-ST4-0
Ultimate load (kN)	12.85	23.72	31.51	59.83
Difference (α) (%)	9.01%	6.98%	0.56%	-0.33%

Table 11 shows the prediction of maximum failure loads calculated from the proposed equations. Although the maximum error was relatively high (around 23 %), the prediction of the maximum failure loads can be acceptable because of several reasons. Firstly, the thickness of the GFM part and UD part are not stable for all specimens. Secondly, although the properties of GFM and CSM GFS are assumed equal together, there are certain differences. However, the properties of GFM cannot be tested separately. Last but not least, although the tightening force was 0 N.m, there was no clearance between the PGFRP plate and CS and SP steel plates, i.e. the washers were slightly fixed by fingers. This can cause small friction forces between PGFRP and steel surfaces and increase the bearing

strength of the GFSs. Table 11 also shows that the predicted failure loads of non-strengthened specimens were closer to the experimental results.

Table 11. Maximum failure loads predicted from the proposed equations and experimental results.

Specimen	Theoretical prediction load (kN)		Experimental load (kN)	Error
	Mode 1	Mode 2		
DL-NS2-0	12.32	-	12.85	-4.13%
DL-NS4-0	25.19	-	23.72	6.20%
DL-ST2-0	-	24.2	31.51	-23.23%
DL-ST4-0	-	48.8	59.83	-18.43%
SL-NS2-0	12.32	-	12.95	-4.86%
SL-NS4-0	25.19	-	22.26	13.17%
SL-ST2-0	-	24.2	28.72	-15.78%
SL-ST4-0	-	48.8	55.39	-11.88%

5. Conclusions

This study investigated the effects of bolt-tightening forces and connection types on the strengths of non-strengthened and GFS-strengthened PGFRP connections. Both double-lap and single-lap specimens were tested using tensile loads. Based on the experimental results, several conclusions were reached, as follows:

- Non-strengthened specimens suffered shear-out failures in their whole sections, whereas a combination of shear-out failures in UD sections and bearing failures in the GFM and GFS sections occurred in GFS-strengthened specimens. For GFS-strengthened specimens, out-of-plane deformations around the bolt positions tended to be larger for single-lap specimens and 0 N.m bolt-tightening force specimens.
- Maximum failure loads increased as tightening forces increased. Increasing levels of maximum failure load approximately linearly changed with increases in the tightening force increment for double-lap specimens, except DL-ST4-20 specimens. However, there was little change in load increases between 5 N.m, 10 N.m, and 20 N.m bolt-tightening forces for single-lap specimens. The linear increase in PGFRP connections' ultimate loads could not be predicted for single-lap connections when bolt-tightening forces increased from 5 N.m to 10 N.m and 20 N.m.
- Maximum failure loads were nearly the same for double-lap and single-lap connections in both non-strengthened and GFS-strengthened specimens. When applying bolt-tightening forces to connections, some trends for increases in maximum failure loads changed. Maximum loads were approximately the same for non-strengthened specimens with 5 N.m and 10 N.m bolt-tightening forces. However, high bolt-tightening forces (20 N.m) could enable a higher maximum load and better performance for double-lap connections (but not single-lap connections) in non-strengthened specimens. There were a few dissimilarities in the maximum loads of GFS-strengthened double-lap and single-lap specimens with two bolts. When GFS-strengthened specimens' bolt number increased to four, double-lap specimens' maximum loads increased by approximately 18.8 %, which was a higher percentage increase than those of single-lap specimens.
- GFSs could improve PGFRP connections' strength when the maximum loads of GFS-strengthened specimens increased from 1.6 to 2.5 times compared with non-strengthened specimens with the same geometries and bolt-tightening forces. Moreover, GFSs could improve PGFRP connections' ductility performances.
- The theoretical equations were proposed to estimate the failure loads of multi-bolted PGFRP connections with 0 tightening forces and proved the acceptable results. Maximum error between theoretical and experimental results was around 23%.

Conflicts of Interest: There are no conflicts of interest.

Funding: This study was supported by the JSPS (Japan Society for the Promotion of Science), KAKENHI (grant

number **22F22066**).

Data availability: The data that support the findings of this study are available from the corresponding author upon reasonable request.

Appendix A. Calculation of bolt tightening force for PGFRP connections

Assume the maximum compression strength ($\sigma_{c,\,max}$) under a washer to be 60 (N/mm^2). In Part 3 of Clarke (1996) [53], there was a report on a series of tests with pinned beam-to-column joints. There was a statement "Bearing pressure is no higher than one-third of the through-thickness crushing strength of the material and in no event higher than 68 N/mm^2". Because the tensile strength and compressive strength of PGFRP are high (426.5 (MPa) and 563.5 (MPa), respectively [33]); therefore, the value of 60 (MPa) for $\sigma_{c,\,max}$ is suitable.

The maximum compression force to be resisted by a washer is $P_{t,\max} = \pi \frac{\left(\phi_s{}^2 - d_s{}^2\right)}{4} \times \sigma_{c,\max} = 13194\ (N)$, where ϕ_s = 19 mm and d_s = 9 mm are the outer and inner diameter of the washer, respectively. The maximum tightening force that should be applied for PGFRP joints can be calculated by the following equation [50,53] $T_{\max} = 0.2 d P_{t,\max} = 21\ (N.m)$, where d is the bolt diameter.

References

[1] H.T. Ali, R. Akrami, S. Fotouhi, M. Bodaghi, M. Saeedifar, M. Yusuf, M. Fotouhi, Fiber reinforced polymer composites in bridge industry, Structures 30 (2021) 774–785

[2] J. Qureshi, A Review of Fibre Reinforced Polymer Structures, Fibers 10 (3) (2022) 27

[3] W. Hu, Y. Li, H. Yuan, Review of Experimental Studies on Application of FRP for Strengthening of Bridge Structures. Adv. Mater. Sci. Eng. 2020 (2020) 8682163

[4] T. Keller, C. Haas, T. Vallée, Structural concept, design and experimental verification of a GFRP sandwich roof structure, J Compos Constr. 12 (4) (2008) 454–468

[5] T. Keller, J. Rothe, J. de Castro, M. Osei-Antwi, GFRP-balsa sandwich bridge deck –concept, design and experimental validation, J Compos Constr. 18 (2) (2014)

[6] T.P. Sathishkumar, S. Satheeshkumar, J. Naveen, Glass fiber-reinforced polymer composites – a review, J Reinf Plast Comp. 33, (2014) 1258-1275

[7] J.R. Correia, Y. Bai, T. Keller, A review of the fire behaviour of pultruded GFRP structural profiles for civil engineering applications, Compos Struct. 127 (2015) 267-287

[8] H. Abdollahiparsa, A. Shahmirzaloo, P. Teuffel, R. Blok, A review of recent developments in structural applications of natural fiber-Reinforced composites (NFRCs), Composites And Advanced Materials 32 (2023) 1-18

[9] X.L. Zhao, L. Zhang, State-of-the-art review on FRP strengthened steel structures, Eng. Struct. 29 (8) (2007) 1808–1823.

[10] H. Nassiraei, P. Rezadoost, Probabilistic analysis of the SCFs in tubular T/Y-joints reinforced with FRP under axial, in-plane bending, and out-of-plane bending loads, Structures 35 (2022) 1078–1097.

[11] S. Reichenbach, P. Preinstorfer, M. Hammerl, B. Kromoser, A review on embedded fibre-reinforced polymer reinforcement in structural concrete in Europe, Constr. Build. Mater. 307 (2021) 124946

[12] J.D. Ortiz, S.S.K. Dolati, P. Malla, A. Nanni, A. Mehrabi, FRP-Reinforced/Strengthened Concrete: State-of-the-Art Review on Durability and Mechanical Effects, Materials 16(5) (2023) 1990

[13] A. Vedernikov, A. Safonov, F. Tucci, P. Carlone, I. Akhatov, Pultruded materials and structures: A review. J. Compos. Mater. 54(26) (2020) 4081-4117

[14] A. Manalo, M. Jackson, Behaviour of pultruded glass fibre reinforced composites guardrail system. Advances in Structural Engineering 21(4) (2018) 545-556

[15] Y.H. Shin, Y.Y. Yoong, H. Hejazi, M.R.R. Saifulnaz, Review on pultruded FRP structural design for building construction. IOP Conference Series: Earth and Environmental Science 357 (2019) 012006

[16] Z. J. Zhang, Y. Bai, X. Xiao, Bonded sleeve connections for joining tubular glass fiber-reinforced polymer beams and columns: experimental and numerical studies. J. Compos. Constr. 22(4) (2018) 04018019.
[17] A. Manalo, T. Aravinthan, A. Fam, M. ASCE, B. Benmokrane, State-of-the-Art review on FRP sandwich systems for lightweight civil infrastructure. J. Compos. Constr. 21 (2017) 1–16
[18] J. Qureshi, A Review of Fibre Reinforced Polymer Bridges, Fibers 11(5) (2023) 40
[19] J. Qureshi, Y. Nadir, S.K. John, Bolted and bonded FRP beam-column joints with semi-rigid end conditions. Compos. Struct. 247 (2020) 112500.
[20] F. Ascione, M. Lamberti, A.G. Razaqpur, S. Spadea, Strength and stiffness of adhesively bonded GFRP beam-column moment resisting connections. Compos. Struct. 160 (2017) 1248–1257.
[21] R.B. Heslehurst, Design and analysis of structural joints with composite materials. Lancaster, PA: DEStech Pub., Inc., 2013.
[22] L. Feo, G. Marra, A.S. Mosallam, Stress analysis of multi-bolted joints for FRP pultruded composite structures. Compos. Struct. 94 (2012) 3769–3780.
[23] N.P. Viet, F.S. Yoresta, Y. Kitane, K. Hashimoto, Y. Matsumoto, Improving the shear strength of bolted connections in pultruded GFRP using glass fiber sheets, Compos. Struct. 255 (2021) 112896
[24] M.A. Masuelli, Introduction of Fibre-Reinforced Polymers—Polymers and Composites: Concepts, Properties and Processes. In Fiber Reinforced Polymers The Technology Applied for Concrete Repair; Masuelli, M.A., Ed.; IntechOpen: London, UK, 2013; ISBN 978-953-51-0938-9
[25] M. Genedy, R. Chennareddy, E.M. Soliman, U.F. Kandil, M.M.R. Taha, Improving shear strength of bolted joints in pultruded glass fiber reinforced polymer composites using carbon nanotubes. J Reinf Plast Comp. 36 (2017) 958-971
[26] E. Soliman, M. Al-Haik, T.M. Reda, On and off-axis tension behavior of fiber reinforced polymer (FRP) composites incorporating multi-walled carbon nanotubes. J Compos Mater. 46 (2012) 1661–1675
[27] K. Sugiyama, R. Matsuzaki, A.V. Malakhov, A.N. Polilov, M. Ueda, A. Todoroki, Y. Hirano, 3D printing of optimized composites with variable fiber volume fraction and stiffness using continuous fiber. Compos Sci Technol. 186 (2020) 107905
[28] Y. Yamanaka, A. Todoroki, M. Ueda, Y. Hirano, R. Matsuzaki, Fiber line optimization in single ply for 3D printed composites. Open J Compos Mater. 6 (4) (2016) 121–131
[29] Mara, V., Haghani, R., Al-Emrani, M.: Improving the performance of bolted joints in composite structures using metal inserts. J Compos Mater. 50, 3001-3018 (2016).
[30] H.J. Park, Effects of stacking sequence and clamping force on the bearing strengths of mechanically fastened joints in composite laminates. Compos. Struct. 53 (2001) 213-221
[31] P.V. Nhut, T.Q. Duc, Y. Matsumoto, The effects of glass fiber sheet lamination on the connection strength of single-bolted pultruded glass fiber reinforced polymer profiles, J. Compos. Mater. 57(20) (2023) 3257-3277
[32] B. Okutan, R. Karakuzu R, The Failure Strength for Pin-Loaded Multi-Directional Fiber-Glass Reinforced Epoxy Laminate, J. Compos. Mater. 36(24) (2002) 2695-2712
[33] P.V. Nhut, F.S. Yoresta, Y. Kitane, K. Hashimoto, Y. Matsumoto, On the strengthening of pultruded GFRP connections using glass fiber sheets: A study on the influence of bolt diameter, Appl. Compos. Mater. 29 (2022) 651–681
[34] P.V. Nhut, T.Q. Duc, Y. Matsumoto, Pin-bearing connection strength of single-bolted pultruded glass fiber-reinforced polymer profiles strengthened by glass fiber sheet, Polym. Compos. 43(8) (2022) 5011-5030
[35] Q.D. Tran, P.V. Nhut, Y. Matsumoto, Multi-Bolted Connection for Pultruded Glass Fiber Reinforced Polymer's Structure: A Study on Strengthening by Multiaxial Glass Fiber Sheets, Polymers 14(8) (2022) 1561
[36] T. Vallée, T. Tannert, R. Meena, S. Hehl, Dimensioning method for bolted, adhesively bonded, and hybrid joints involving Fibre-Reinforced-Polymers, Compos. Part B Eng. 46 (2013) 179–187
[37] Y.G. Lee, E. Choi, S.J. Yoon, Effect of geometric parameters on the mechanical behavior of PFRP single bolted connection, Compos. B. Eng. 75 (2015) 1-10
[38] A.M.G. Coelho, J.T. Mottram JT, A review of the behaviour and analysis of bolted connections and joints in pultruded fibre reinforced polymers, Mater. Des. 74 (2015) 86-107
[39] T.A. Tajeuna, F. Légeron, S. Langlois, P. Labossière, M. Demers, Effect of geometric parameters on the behavior of bolted GFRP pultruded plates, J. Compos. Mater. 50(26) (2016) 3731-3749
[40] Y. Zhu, H. Zhu, V. Gribniak, Analyzing the Sample Geometry Effect on Mechanical Performance of Drilled

GFRP Connections, Materials 15 (2022) 2901
[41] R. Prabhakaran, S. Devara, Z. Razzaq, The effect of fiber orientation angle on the unnotched, open hole, and pin-loaded strength of a pultruded composite. In: Proc. 51st Annual Conf. of the Composites Inst., Society of the Plastics Industry, Washington DC, (1996) 1–15
[42] R.L. Yuan, C.J. Liu, Experimental characterization of FRP mechanical connections. In: Proc. 3rd Inter Conf. on advanced composite materials in bridges and structures. The Canadian Society for Civil Engineers, (2000) 103–10
[43] G.J. Turvey, Single-bolt tension joint tests on pultruded GRP plate: effects of tension direction relative to pultrusion direction, Compos Struct. 42(4) (1998) 341–351
[44] M. Bazli, H. Ashrafi, A. Jafari, X-L. Zhao, R.K.S. Raman, Y. Bai, Effect of Fibers Configuration and Thickness on Tensile Behavior of GFRP Laminates Exposed to Harsh Environment, Polymers 11 (2019) 1401
[45] M.R.M. Asyraf, A. Syamsir, N.M. Zahari, A.B.M. Supian, F. Usman, Z. Itam, Effect of Stacking Sequence on Long-Term Creep Performance of Pultruded GFRP Composites, Polymers 14 (2022) 4064
[46] H. Xin, Y. Liu, A.S. Mosallam, J. He, A. Du, Evaluation on material behaviors of pultruded glass fiber reinforced polymer (GFRP) laminates, Compos. Struct. 182 (2017) 283-300
[47] J. Gao, Q. Zhao, J. Liu, L. Chen, Effect of transverse clamping force on the tensile behavior of a novel pultruded carbon fiber–reinforced polymer joint: Fatigue test, Adv. Struct. Eng. 23(7) (2020) 1413-1422
[48] I.K. Giannopoulos, D.D. Dawes, K.I. Kourousis, M. Yasaee, Effects of bolt torque tightening on the strength and fatigue life of airframe FRP laminate bolted joints, Compos. B: Eng. 125 (2017) 19-26
[49] J. Liu, T. Guo, Y. Wei, L. Wang, X. Zou, Investigation of the effect of pre-tightening forces on bolted connection for FRP-steel joints, Case Stud. Constr. Mater. 19 (2023) e20348
[50] J. Qureshi, Y. Nadir, S.K. John, Cyclic Response of Bolted and Hybrid Pultruded FRP Beam-Column Joints between I-Shaped Sections, Fibers. (2021) 9(11):66
[51] P.A. Smith, M.F. Ashby, K.J. Pascoe, Modelling Clamp-Up Effects in Composite Bolted Joints, J. Compos. Mater. 1987, 21, 878–897
[52] American Composites Manufacturer Association (ACMA) ASCE, Pre-Standard for load and resistance factor design (LRFD) of pultruded fiber polymer (FRP) structures (Final)", (2010).
[53] J.L. Clarke, Structural Design of Polymer Composites—EUROCOMP Design Code and Handbook; CRC Press: Boca Raton, FL, USA, 1996.